What are Marine Ecological Time Series telling us about the ocean? A status report

[Individual Chapter (PDF) download]

The full report (all chapters and Annex) is available online at:

http://igmets.net/report

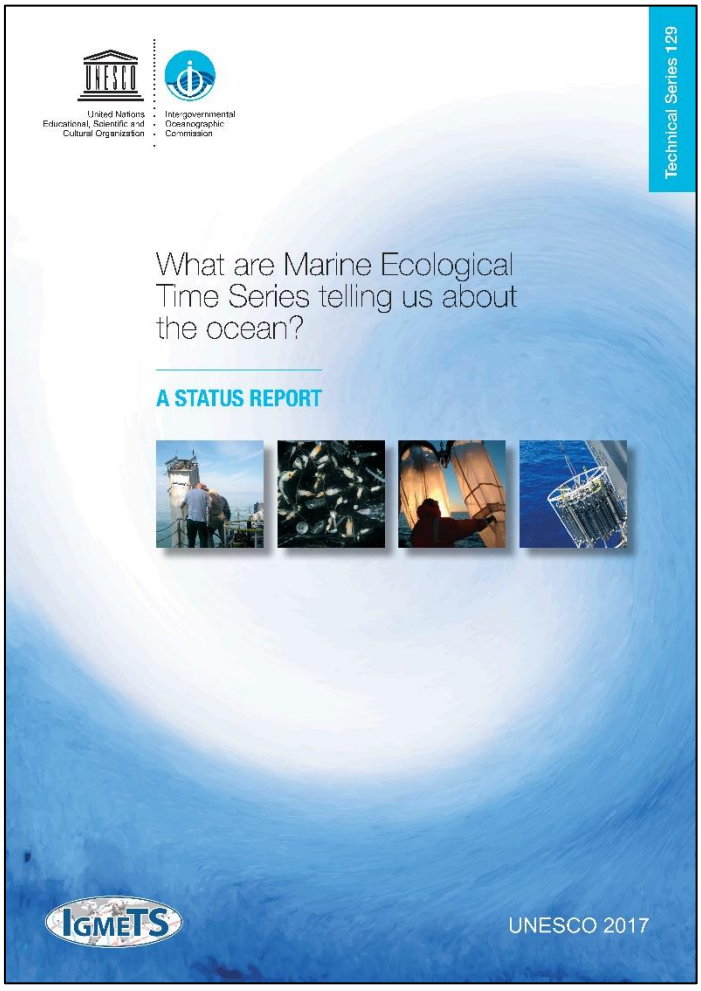

This page intentionally left blank

to preserve pagination in double-sided (booklet) printing

7 Indian Ocean

Peter A. Thompson, Todd D. O'Brien, Kirsten Isensee, Laura Lorenzoni, and Lynnath E. Beckley

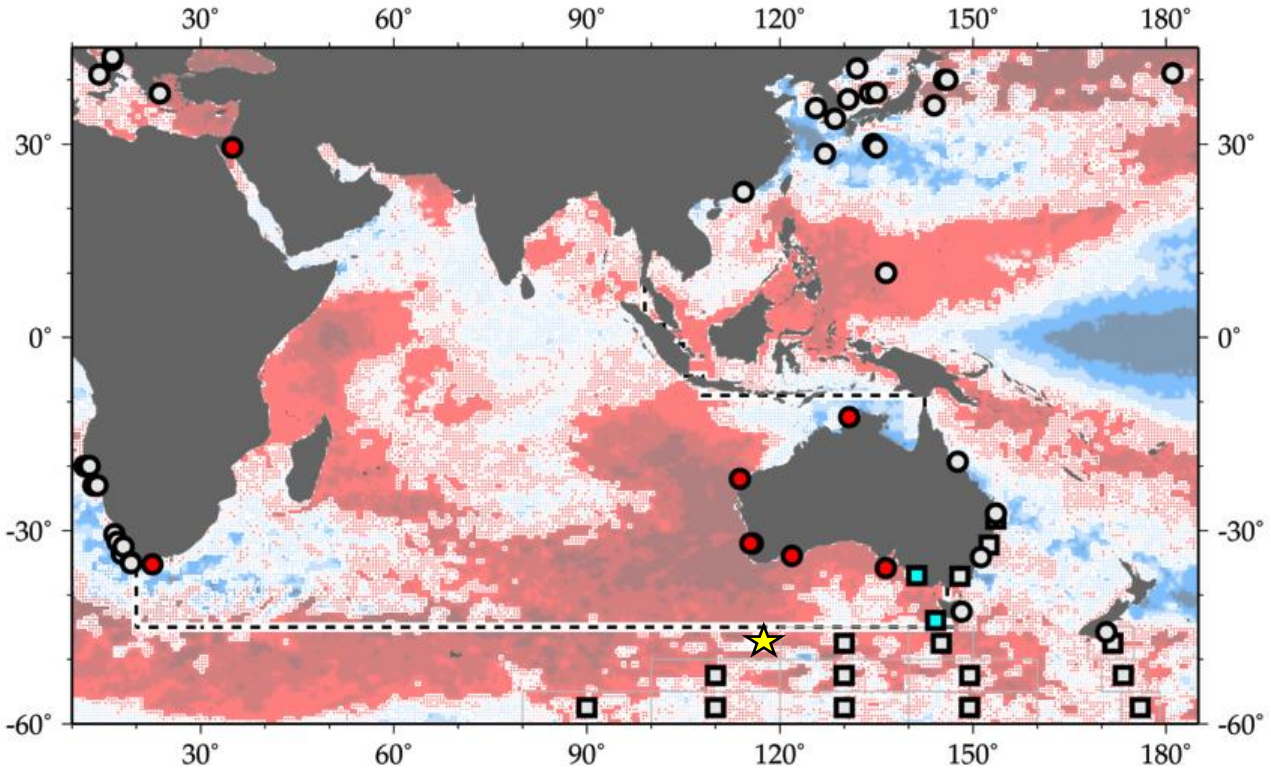

Figure 7.1. Map of IGMETS-participating Indian Ocean time series on a background of a 10-year time-window (2003–2012) sea surface temperature trends (see also Figure 7.3). At the time of this report, the Indian Ocean collection consisted of 10 time series (coloured symbols of any type), of which two were Continuous Plankton Recorder surveys (blue boxes) and one was estuarine (yellow star). Dashed lines indicate boundaries between IGMETS regions. Uncoloured (gray) symbols indicate time series being addressed in a different regional chapter (e.g. Southern Ocean, North/South Pacific, South Atlantic). See Table 7.3 for a listing of this region's participating sites. Additional information on the sites in this study is presented in the Annex.

Participating time-series investigators

Uli Bathmann, Frank Coman, Claire Davies, Ruth Eriksen, Mitsuo Fukuchi, Amatzia Genin, Graham Hosie, Jenny Huggett, Takahashi Kunio, Felicity McEnnulty, Anthony Richardson, Malcolm Robb, Don Robertson, Karen Robinson, Yonathan Shaked, Anita Slotwinkski, Peter A. Thompson, Mark Tonks, and Julian Uribe-Palomino

This chapter should be cited as: Thompson, P. A., O'Brien, T. D., Isensee, K., Lorenzoni, L., and Beckleyiebe, L.E. 2017. Indian Ocean. I*n* What are Marine Ecological Time Series telling us about the ocean? A status report, pp. 113–132. Ed. by T. D. O'Brien, L. Lorenzoni, K. Isensee, and L. Valdés. IOC-UNESCO, IOC Technical Series, No. 129. 297 pp.

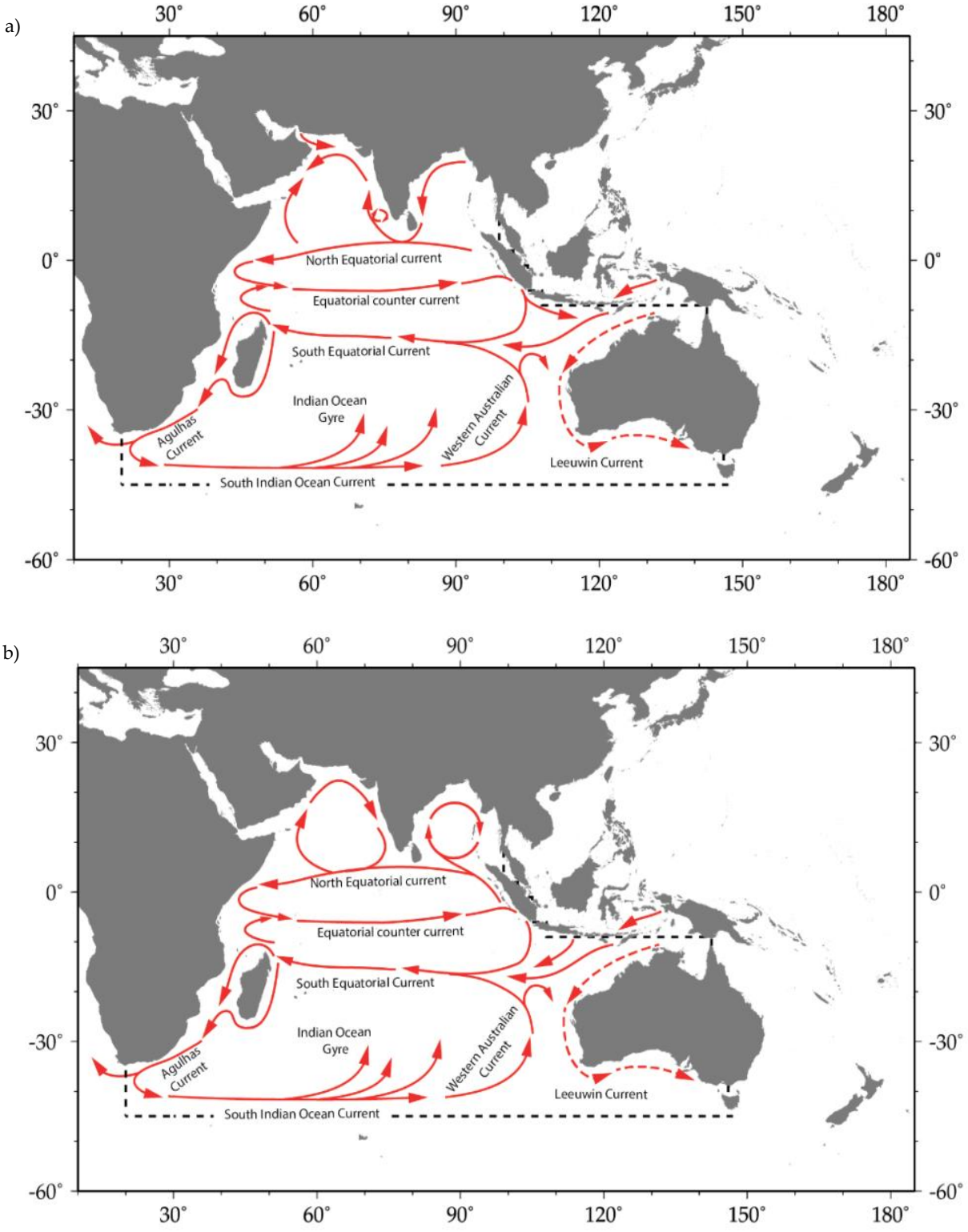

Figure 7.2. Major Indian Ocean Currents (adapted from Schott *et al.*, 2009). a) Late Northeast Monsoon (March–April); b) Late Southwest Monsoon (September–October).

7.1 Introduction

With a southern boundary historically ranging from 60°S to the Antarctic continent, the Indian Ocean is the fourth largest ocean with an area of up to 74 million km^2. As the IGMETS analysis required non-overlapping ocean regions for its spatiotemporal trend calculations, and likewise could only assign each time series to a single region, a boundary of 45°S was used to define and separate the Indian Ocean region from the Southern Ocean region. This modified area, ca. 7800 km wide and stretching from about 25°N to 45°S, had an area of 56.8 million km^2. Unlike the North Atlantic and North Pacific oceans, the Eurasian landmass in the north precludes high-latitude cooling of surface waters in the northern Indian Ocean. There is, however, some low-latitude exchange of water between the Pacific and Indian oceans via the Indonesian Throughflow. The only large shelf areas are the shallow seas north of Australia, which are regions of strong tidal dissipation. There are a number of significant meridional ridges and several deep basins extending below 5000 m. Within the Indian Ocean, there are several marginal seas, gulfs, and bays, with the Indian subcontinent separating the two most prominent, namely the Arabian Sea and the Bay of Bengal. The Arabian Sea, extending between roughly 10–23°N and 51–74°E, reaches depths >3000 m over most of its area and has two important regions: the Gulf of Aden to the southwest, connecting with the Red Sea, and the Gulf of Oman to the northwest, which connects with the Persian Gulf. The Bay of Bengal, which occupies an area of 2 172 000 km^2, receives input from a number of rivers, the most important being the Ganges–Brahmaputra river system.

This river system delivers large quantities of sediment to the Bengal Fan, which causes depth in the Bay of Bengal to decrease gradually from 4000 m south of Sri Lanka to ≤ 2000 m at 18°N (Tomczak and Godfrey, 2003; Galy *et al*., 2007). The circulation of the northern Indian Ocean is dominated by the monsoons and their seasonal switching between strong southwest winds during June–September and weaker northeast winds in October–March (Talley *et al*., 2011). The winds drive a reversal of the surface currents in both the Bay of Bengal and Arabian Sea (Figure 7.2). In particular, the western boundary current in the Arabian Sea, the Somali Current, flows northward in boreal summer and then reverses to flow largely southward in boreal winter. The summer pattern of wind and current stimulates a strong current and upwelling along the coast from Somalia to Oman (Beal and Chereskin, 2003). The northern hemisphere summer monsoons provide intense rainfall between 10–20°N and 70–120°E, which is of considerable importance to agriculture in the region. The tropical southern Indian Ocean typically has a wet monsoon between November and March that produces rainfall around 5–10°S and across the entire basin. In contrast, the austral winter (April–October) monsoon creates some upwelling along the west coasts of Java and Sumatra (Wyrtki, 1962) that tends to be strongest during El Niño events (Susanto *et al*., 2001). The Agulhas Current is a strong western boundary current that transports 70 Sv poleward at 31°S, with flow that varies from 9 to 121 Sv at velocities of up to 2 m s^{-1} at 35°S (Boebel *et al*., 1998; Bryden *et al*., 2005). As the Agulhas Current reaches the southern tip of Africa, most of the water is reflected to the east by the "westerly wind drift" (Lutjeharms and van Ballegooyen, 1988) along the subtropical front (STF). However, a modest volume of warm, saline Indian Ocean water is transported into the South Atlantic through the Agulhas leakage. It has been suggested that the Agulhas leakage is an important component of the climate system (Beal *et al*., 2011). The STF is a long narrow feature stretching from the east coast of South America, through the South Atlantic, Indian, and South Pacific oceans to the west coast of South America. It separates the warm, salty subtropical waters from colder, fresher Antarctic waters. The STF region is high in eddy kinetic energy and develops large coccolithophorid blooms in summer (Balch *et al*., 2011, 2016).

The Leeuwin Current forms the eastern boundary current for the Indian Ocean and is unusual, as it flows poleward albeit with much less volume (ca. 5 Sv) than the Agulhas Current (Godfrey and Ridgway, 1985). The poleward flow of warm, fresher water typically peaks in May or June (Figure 7.2). The buoyant Leeuwin Current also flows eastward through the Great Australian Bight along the south coast of Australia in winter suppressing upwelling along its length (Ridgway and Condie, 2004). The oligotrophic southern Indian Ocean central gyre has previously been estimated to be growing in size in response to climate drivers (Jena *et al*., 2013; Signorini *et al*., 2015).

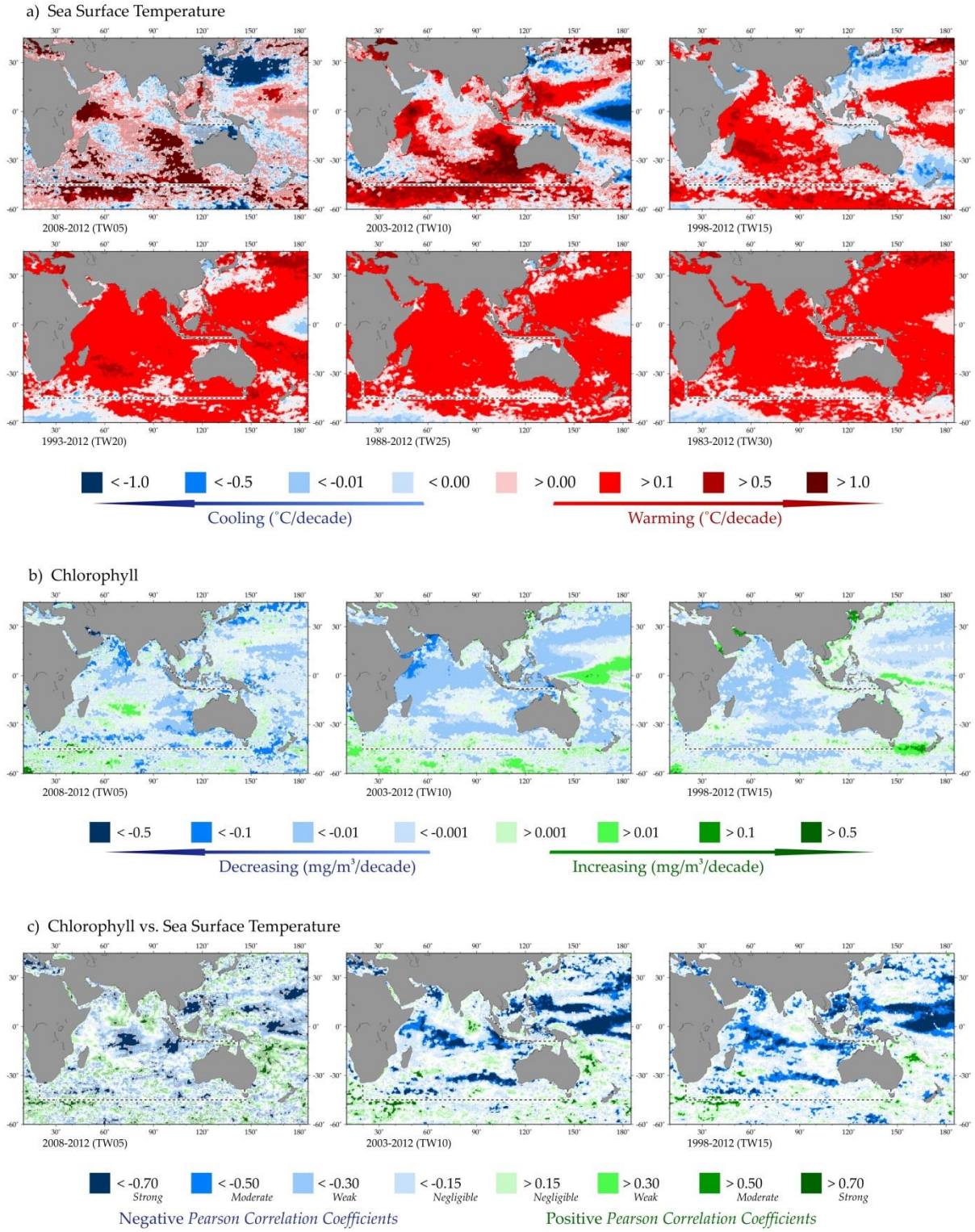

Figure 7.3. Annual trends in Indian Ocean sea surface temperature (SST) (a) and sea surface chlorophyll (CHL) (b), and correlations between chlorophyll and sea surface temperature for each of the standard IGMETS time-windows (c). See "Methods" chapter for a complete description and methodology used.

7.2 General patterns in temperature and phytoplankton biomass

For the entire Indian Ocean, the overwhelming trend in temperature has been upwards (Figure 7.3; Table 7.1). During 1983–2012, ca. 98% of the Indian Ocean was warming, 81.9% showed a significant temperature increase > 0.1 and ≤ 0.5°C decade^{-1} (Table 7.1). This was the greatest proportion of warming for any ocean on the planet (Chapter 10) and is associated with a range of climate cycles including the relatively long positive phase of the Interdecadal Pacific Oscillation (Han *et al*., 2014). Over this same time-period, only 0.5% of the Indian Ocean was found to be significantly cooling (Table 7.1).

The analysis over multiple 5-year time-windows shows that temperature changes were more rapid and more variable over shorter intervals (Table 7.1; Figure 7.3). For example, 19.3% of the Indian Ocean was warming at a high rate of > 1.0°C decade^{-1} over the 5-year window (2008–2012), but this rate was not observed over the 15-year time-window (1998–2012). Between 2008 and 2012, the statistically significant rates of warming ranged from –1.0 to +1.0°C decade^{-1} (Figure 7.4a). Over the longer temporal window from 1983 to 2012, these rates tended to be 5–10-fold less variable ranging from –0.5 to +0.5°C decade^{-1} (Figure 7.4b). Notwithstanding the influence of statistics itself, the declining variability in the rate of temperature changes suggests that the shorter-term climate cycles predominately have periods that are less than 30 years. Consider that the proportion of the Indian Ocean warming rose 0.75% year^{-1} as the time series lengthened from 0 to 20 years, then only 0.23% year^{-1} as the time series was extended another 10 years (Table 7.1). The slowing in the spatial expansion and consolidation of the rate at an intermediate value suggests that the variability associated with shorter-term climatic signals in the Indian Ocean (e.g. Indian Ocean Dipole, El Niño Southern Oscillation) is reduced when using a linear model and more than 20 years of data.

More than 79% of the Indian Ocean experienced a decline in surface chlorophyll *a* over the 15-year time-period from 1998 to 2012, while only 20.3% had an increase (Figure 7.3). The proportion of the Indian Ocean experiencing a decline in chlorophyll *a* was the greatest for any ocean (Table 7.1; Chapter 10) and highly correlated with warming (Figure 7.3). The main areas of cooling and increasing chlorophyll *a* were associated with just four regions: (i) the Arabian Sea and surrounding areas (Red Sea and Persian Gulf), (ii) along the south-west coasts of Sumatra and the Sunda Islands, (iii) south from Madagascar, and (iv) along the subtropical front (STF) at ca. 40–45°S (Figure 7.3). The spatial pattern of increasing chlorophyll *a* tended to vary depending on the temporal window considered, but was arguably most consistent along the STF.

There was significant cooling in the Red Sea, Arabian Sea, Persian Gulf, and along the coasts of Oman and Yemen between 1998 and 2012 (Figure 7.3). Almost none of this regional cooling was evident over the longer 30-year time-window, suggesting that it was strongly influenced by relatively short climatic cycles such as the Indian Ocean Dipole (IOD) and ENSO. It is also possible that this regional cooling was caused by greater seasonal upwelling associated with an increased frequency of stronger IOD and ENSO events that were predicted as a response to climate change (Cai *et al*., 2015).

The Arafura and Timor seas north of Australia also trended colder during 1998–2012. It is probable that this colder trend resulted from the strong positive IOD in 2011 and 2012 and a weakening La Niña (Meyers *et al*., 2007). The IOD primarily affects the pelagic ecology of this region through upwelling favourable winds (Currie *et al*., 2013; Kämpf, 2015).

There was a relatively broad region of cooling off south-east Africa below Madagascar where the Southeast Madagascar and Agulhas currents normally transport considerable amounts of warm water southward (Yamagami and Tozuka, 2015). Although the Southeast Madagascar Current flow is associated with ENSO, this cooling was consistent throughout the different time-windows (Figure 7.3), suggesting a longer-term effect. The source of this surface cooling is unclear. A possibility is the multidecadal rise in subtropical wind stress and increased Southeast Madagascar Current flow (Backeberg *et al*., 2012). The increased South Madagascar Current resulted in a substantial rise in eddy kinetic energy and, in turn, promoted greater vertical mixing for this region (Backeberg *et al*., 2012). Similarly, the region showed mesoscale patches of warming, consistent with increased Agulhas and Southeast Madagascar Current flow.

Table 7.1. Relative spatial areas (% of the total region) and rates of change within within the Indian Ocean region that are showing increasing or decreasing trends in sea surface temperature (SST) for each of the standard IGMETS time-windows. Numbers in brackets indicate the % area with significant ($p < 0.05$) trends. See "Methods" chapter for a complete description and methodology used.

Latitude-adjusted SST data field surface area = 56.8 million km^2	**5-year** (2008–2012)	**10-year** (2003–2012)	**15-year** (1998–2012)	**20-year** (1993–2012)	**25-year** (1988–2012)	**30-year** (1983–2012)
Area (%) w/ increasing SST trends ($p < 0.05$)	**66.7%** (*26.4%*)	**76.0%** (*47.4%*)	**82.6%** (*58.1%*)	**96.7%** (*87.9%*)	**96.2%** (*89.4%*)	**97.8%** (*91.9%*)
Area (%) w/ decreasing SST trends ($p < 0.05$)	33.3% (*4.2%*)	24.0% (*4.5%*)	17.4% (*4.6%*)	3.3% (*0.8%*)	3.8% (*0.7%*)	2.2% (*0.5%*)
> 1.0°C decade^{-1} warming ($p < 0.05$)	24.8% (*19.3%*)	7.8% (*7.8%*)	0.0% (*0.0%*)	0.0% (*0.0%*)	0.0% (*0.0%*)	0.0% (*0.0%*)
0.5 to 1.0°C decade^{-1} warming ($p < 0.05$)	18.8% (*6.1%*)	19.0% (*18.3%*)	6.6% (*6.5%*)	2.9% (*2.9%*)	0.1% (*0.1%*)	0.0% (*0.0%*)
0.1 to 0.5°C decade^{-1} warming ($p < 0.05$)	18.1% (*0.9%*)	38.5% (*20.9%*)	**60.3%** (*49.2%*)	**86.2%** (*83.3%*)	**84.2%** (*83.3%*)	**82.2%** (*81.9%*)
0.0 to 0.1°C decade^{-1} warming ($p < 0.05$)	5.0% (*0.0%*)	10.7% (*0.5%*)	15.7% (*2.3%*)	7.6% (*1.7%*)	11.9% (*6.0%*)	15.6% (*10.0%*)
0.0 to –0.1°C decade^{-1} cooling ($p < 0.05$)	4.1% (*0.0%*)	8.7% (*0.1%*)	7.1% (*0.1%*)	2.0% (*0.1%*)	2.7% (*0.1%*)	1.7% (*0.1%*)
–0.1 to –0.5°C decade^{-1} cooling ($p < 0.05$)	15.0% (*0.5%*)	12.7% (*2.4%*)	9.7% (*3.9%*)	1.2% (*0.6%*)	1.1% (*0.6%*)	0.5% (*0.3%*)
–0.5 to –1.0°C decade^{-1} cooling ($p < 0.05$)	8.7% (*1.5%*)	2.3% (*1.8%*)	0.6% (*0.6%*)	0.1% (*0.1%*)	0.0% (*0.0%*)	0.0% (*0.0%*)
> –1.0°C decade^{-1} cooling ($p < 0.05$)	5.5% (*2.2%*)	0.3% (*0.2%*)	0.1% (*0.1%*)	0.0% (*0.0%*)	0.0% (*0.0%*)	0.0% (*0.0%*)

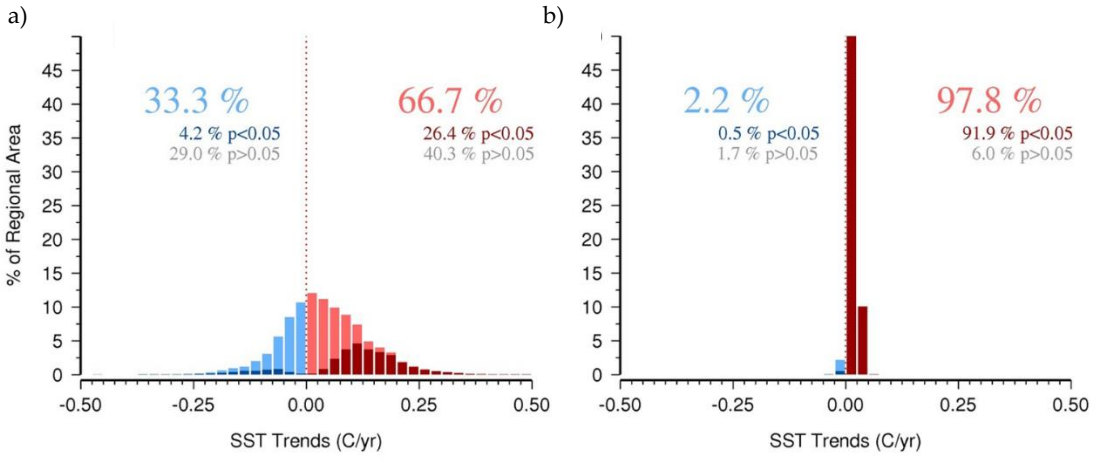

Figure 7.4. The range of SST trends observed over different temporal windows in the Indian Ocean. (a) From 2008 to 2012, 33.3% (66.7%) of the area was cooling (warming); while 4.2% (26.4%) was cooling (warming) significantly ($p < 0.05$). Rates of cooling and warming ranged from –0.50 to +0.50°C year^{-1}. (b) Over the longer-term from 1983 to 2012, the rates of temperature change were much more constrained, ranging from –0.05 to 0.075°C year^{-1}. Over this 30-year period, only 2.2% (97.8) of the area was cooling (warming), while 0.5% (91.9%) was cooling (warming) significantly ($p < 0.05$).

It is suggested that stronger increasing eddy kinetic energy observed across the Agulhas retroflection (Swart *et al*., 2015) added to this spatial mosaic of mesoscale variability in warming and cooling trends. The spatial pattern of patchy cooling extended across the entire Indian Ocean at ca. 40°S, suggesting that this effect can be seen a long way eastward along the edge of the STF. There was also cooling south of Africa between 20–60°E and 50–60°S. This probably relates to the long-term positive trend in the SAM (Swart *et al*., 2015), which increases the westerly flow along 60°S, decreasing SST to lower-than-normal values (Lovenduski and Gruber, 2005; Verdy *et al*., 2006).

Between 1998 and 2012, there were upward trends in chlorophyll *a* within the southern Red Sea, Persian Gulf, and patches through the Gulf of Oman and Arabian Sea off the coasts of Yemen and Oman that largely coincide with regions of declining SST. The latter are regions of upwelling that are known to respond to stronger winds during the summer southwest monsoon season (Yi *et al*., 2015). The trends in chlorophyll *a* are clearly dependent on the temporal window selected with downward trends for most of this region over the shorter 10-year window from 2003 to 2012. Over the shortest temporal window from 2008 to 2012, trends in chlorophyll *a* were mixed across the region, although quite strongly negative in the Persian Gulf (Figure 7.3). A 60-year reconstruction of summer blooms based on SST suggested that regional summer chlorophyll *a* concentrations might have peaked during the very strong upwelling of 1966 (Roxy *et al*., 2016).

The rise in chlorophyll *a* from 1998 to 2012 along the coasts of Java and Sumatra, weakly through the Timor and Arafura seas, and into the Gulf of Carpentaria was in regions that respond to positive ENSO and IOD conditions (Currie *et al*., 2013). These climatic indices were positive on average and trending positive throughout this 15-year period. Indeed, the 15-year period started with predominant El Niño episodes and progressed to include several moderate-to-strong La Niña events in the latter half. The mechanisms potentially driving an increase in chlorophyll *a* across this diverse region include upwelling favorable winds off Java and Sumatra, increased runoff into the Gulf of Carpentaria, and greater interocean exchange from the Pacific to the Indian Ocean for the shallow Arafura and Timor seas.

There were patches of increased chlorophyll *a* southeast of Africa and south of Madagascar observed across all three temporal windows. These patches were also evident across the Indian Ocean sector near the STF. In these regions, the patchy spatial distribution of the increasing chlorophyll *a* has a strong resemblance to the spatial pattern of increased SSH and increasing eddy kinetic energy observed during 1993–2009 (Backeberg *et al*., 2012). Thus, the spatial nature of the increased phytoplankton in this region can be hypothesized to be associated with increased eddy pumping (Falkowski *et al*., 1991). Eastward, along the STF, it is likely that eddies with increased deep mixing at this convergence zone have created this mosaic of increased and decreased chlorophyll *a*. The most pronounced increases in phytoplankton along the Indian Ocean sector of the STF were observed close to Tasmania, where the STF interacts with a strengthening East Australian Current (Figure 7.3).

Mostly at latitudes > 45°S, although occasionally closer to the equator, there were scattered regions where chlorophyll *a* was trending upwards. A positive SAM has been associated with changes in the ocean meridional overturning circulation, including increased upwelling of nutrient-rich waters in the region of 60°S (Hall and Visbeck, 2002), as well as a shallower surface mixed layer depth (Lovenduski and Gruber, 2005). The ENSO also exerts an influence on phytoplankton in this region; for example, when a positive SAM aligns with a positive ENSO event, eddy kinetic energy increases significantly (Langlais *et al*., 2015). Between 35 and 60°S, the spatial patterns of SST and chlorophyll *a* trends were quite consistent across all temporal windows examined. However, during 2003–2012, the warming and greening was broader, but patchier. The trend and average condition of both ENSO and SAM cycles were positive during these 10 years, factors that have been previously linked to increased chlorophyll *a* in these regions (Lovenduski and Gruber, 2005). During this time, the deeply mixed surface layer of the Subantarctic Zone (SAZ) and Polar Front Zone (PFZ) apparently became more conducive for phytoplankton growth. The mechanism for this response is hypothesized to be the upwelling of iron or shallowing of the surface mixed layer (Carranza and Gille, 2015).

During 2008–2012, the south Indian central gyre cooled, and a broad increase in chlorophyll *a* was also observed in that area. The explanation for this strong reversal of the longer-term trend is not evident at this point and may merit further investigation. Indeed, most research has shown the subtropical gyres to be expanding, warming, and declining in phytoplankton (Jena *et al*., 2013; Signorini *et al*., 2015).

Table 7.2. Five-year trends (TW05, 2008–2012) in the time series of observations from *in situ* sites in the South Pacific (not including Continuous Plankton Recorder sites).

Site-ID	Lat (°E) Long (°S)	SST	S	Oxy	NO3	CHL	Cope-pods	Dia.	Dino.	Dia.: Dino.
au-40114 SO CPR Aurora	19.18 147.37	+	-	*n/a*	*n/a*	-	-	*n/a*	*n/a*	*n/a*
au-40205 AusCPR MEAD Line	27.20 153.33	*n/a*	*n/a*	*n/a*	*n/a*	*n/a*	*n/a*	*n/a*	*n/a*	*n/a*
au-50102 IMOS NRS – Darwin	34.05 151.15	*n/a*	*n/a*	*n/a*	*n/a*	*n/a*	*n/a*	*n/a*	*n/a*	*n/a*
au-50103 IMOS NRS – Esperance	42.35 148.14	+	-	-	-	+	+	-	-	-
au-50104 IMOS NRS – Kangaroo Island	36.5 73.0	-	-	-	-	-	-	-	-	-
au-50106 IMOS NRS – Ningaloo	23.1 70.47	*n/a*	*n/a*	*n/a*	*n/a*	*n/a*	*n/a*	*n/a*	*n/a*	*n/a*
au-50108 IMOS NRS – Rottnest Island	4.8 82.00	*n/a*	-	*n/a*	*n/a*	-	*n/a*	-	*n/a*	-
il-10101 Gulf of Eilat NMP Station A	16.00 75.00	-	-	-	-	-	-	-	-	-
za-30202 ABCTS Mossel Bay	11.99 78.97	*n/a*	*n/a*	*n/a*	*n/a*	*n/a*	*n/a*	-	*n/a*	*n/a*

$p > 0.05$ negative positive

7.3 Trends from *in situ* time series

There is a dire paucity of ecological long-term time-series data openly available for the Indian Ocean (Figure 7.5). Most of the small number of time series extend for < 10 years. The lack of these data makes it nearly impossible to even describe the current status of the ecosystem and its pelagic biota or their temporal trends at the basin scale.

The most heavily sampled region is the coastal zone around Australia, extending from Darwin (12°S 131°E) to Tasmania (42°S 148°E), mostly in the Longhurst biogeographical province No. 2 (Longhurst, 2007), the Indonesian and Australian Coastal Province (Figure 7.6). The footprint of these stations indicates that they can represent temperature and chlorophyll *a* temporal trends across a large portion of the adjacent shelf (Oke and Sakov, 2012; Jones *et al*., 2015). Within the Australian portion of this province, the Leeuwin Current (LC) is a strong influence bringing warm, low-salinity, silicate-rich water southward from the tropics (Thompson *et al*., 2011). During 2008–2012, two stations, Esperance and Rottnest Island (Table 7.2), showed the most signs of greater LC effects, such as increasing SST, decreases in salinity, declining dissolved oxygen (DO), and fewer diatoms (Figure 7.5). Copepod biomass rose at both these sites, as did chlorophyll *a* at Esperance (Figure 7.5). The latter result is in strong contrast to the general trend of declining chlorophyll *a* within this region (Figure 7.3), possibly reflecting a more localized effect at this near-shore station or the increased intrusion of productive STF eddies onto the shelf (Schodlok *et al*., 1997; Cresswell and Griffin, 2004). The nearby estuarine site in the Swan River had 10-year trends of increasing temperature, chlorophyll *a*, and DO, but declines in phosphate and dinoflagellates. These are strongly influenced by declining rainfall (Thompson *et al*., 2015). The Kangaroo Island site is also located in Longhurst No. 2 near the extreme eastern end of the Indian Ocean. This site is influenced by wind-driven upwelling with weak links to ENSO and SAM (Nieblas *et al*., 2009). The site showed declines in nitrate, zooplankton, diatoms, and the diatom/dinoflagellate ratio, with a modest increase in salinity from 2008 to 2012 (Table 7.2; Figure 7.5). The declines in the proportion of diatoms and diatom/dinoflagellate were found at three stations along the bottom of Australia. Consistent with satellite data, the time series from the Gulf of Eilat site in the northern Red Sea showed a strong increase in temperature and dissolved oxygen and a weak increase in chlorophyll *a* between 2008 and 2012 (Table 7.2).

Salinity, nitrate, phosphate, and silicate all trended down over the 5-year time-window between 2008 and 2012. The only other time series currently available from the Indian Ocean is at the western extreme at Mossel Bay on the Agulhas Bank. This is one of two regions on the Bank that have been sampled since 1979 (Hutchings *et al*., 1995). There was a strong negative trend in zooplankton biomass over the 15-year time-window from 1998 to 2012 (Table 7.2).

In summary, across the few *in situ* time series available for the Indian Ocean, the trends in temperature were generally upward, while salinity trended down. Trends in nitrate were also generally downward, but other nutrients and biology were variable. These results suggest that local or shorter-term complexities in the oceanography are important in determining ecosystem responses even in the presence of a pervasive warming trend.

7.4 Consistency with previous analysis

Over the 15-year time-period from 1998 to 2012, the average IOD and ENSO indices were positive and trending positive, while the SAM was positive, but trending slightly more negative. These shorter climatic cycles impact most significantly on the Indian Ocean environment and its ecology. The environmental impacts tend to oscillate, with some level of periodicity associated with these climate cycles (Eccles and Tziperman, 2004; Yamagata *et al*., 2003; Fogt *et al*., 2009).

The ENSO climatic driver is the primary source of inter-annual variability in climate throughout most of the Pacific Ocean and portions of the Indian Ocean (Weiqing *et al*., 2014; Cai *et al*., 2015). It is a coupled ocean and atmosphere cycle that can be represented by the Southern Oscillation Index (SOI) based on the difference in surface air pressure between Tahiti and Darwin (Australia).

A persistently positive SOI (lower pressure over Darwin than Tahiti) is a La Niña event. During such an event, strong Pacific trade winds and surface currents push warm water in the tropics westward causing increasing SST, increased steric height, greater rainfall, and reduced SSS. The increased volume of seawater transported from the Pacific Ocean to the Indian Ocean by a La Niña event has been estimated at 5 Sv (Meyers, 1996), and this contributes to a stronger Leeuwin Current.

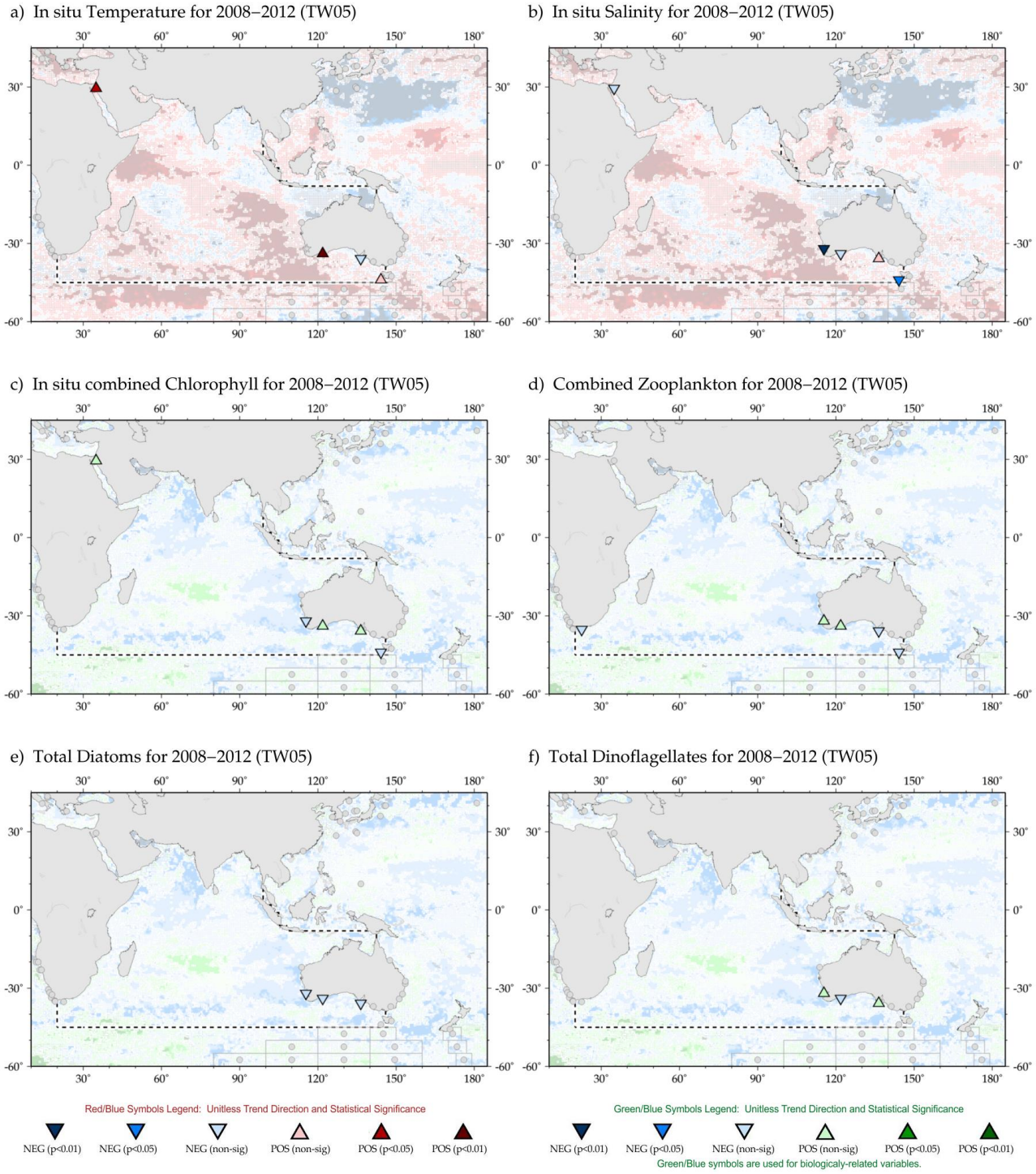

Figure 7.5. Map of Indian Ocean region time-series locations and trends for select variables and IGMETS time-windows. Upward-pointing triangles indicate positive trends; downward triangles indicate negative trends. Gray circles indicate time-series sites that fell outside of the current study region or time-window. Additional variables and time-windows are available through the IGMETS Explorer (http://IGMETS.net/explorer). See "Methods" chapter for a complete description and methodology used.

The intensity of the IOD is represented by an anomalous SST gradient between the western equatorial Indian Ocean (50–70°E and 10°S–10°N) and the southeastern equatorial Indian Ocean (90–110°E and 10°S–0°N; Saji *et al*., 1999). This gradient is also known as the Dipole Mode Index (DMI). Typically, significant anomalies appear around June, intensify in the following months, and peak in October. During a positive IOD, anomalously strong winds push warm water west towards Africa, decreasing upwelling in that region, and increasing upwelling (lower SST) along the west coast of Sumatra (Alory *et al*., 2007). A positive IOD is also associated with reduced rainfall in Indonesia and northern Australia. Lastly, during a positive Southern Annular Mode (SAM) event, the southern hemisphere westerly winds tend to move farther southward and increase in intensity (Gong and Wang, 1999; Thompson *et al*., 2000). This results in stronger cold water upwelling at high latitudes, anomalous downwelling around 45°S, and a strengthening of the Antarctic Circumpolar Current (Hall and Visbeck, 2002; Oke and England, 2003). There is significant temporal variability in the SAM, but over the last 50+ years, the SAM index has been positive and on the rise (Thompson *et al*., 2000; Abram *et al*., 2014); this rise has been linked to anthropogenic factors that include ozone depletion (Fyfe *et al*., 1999).

The analyses presented here are broadly consistent with previous work in the Indian Ocean in terms of warming and the biological responses. However, there are also some discrepancies. For example, some studies of phytoplankton biomass using remote sensing have reported declines in parts or most of the north Indian Ocean (Gregg and Rousseaux, 2014; Roxy *et al*., 2016), in the Equatorial Indian Ocean (Gregg and Rousseaux, 2014), and in the central gyre of the southern Indian Ocean (Jena *et al*., 2013; Signorini *et al*., 2015). The choice of time and space scale used in the analysis clearly influences the result. Shorter time-periods are prone to detecting responses to shorter climatic cycles. For example, the 5-year analysis presented here showed increasing chlorophyll *a* in the south Indian Ocean central gyre (Longhurst 33) during 2008–2012, suggesting a possible link to an intermediate climate cycle (e.g. ENSO or IOD). In addition, the analysis of trends at smaller spatial scales is clearly demonstrating important patterns that can be overlooked if averaging at a larger spatial scale.

Long-term changes to sea surface temperature, surface salinity, and dissolved oxygen in the Indian Ocean have all been previously investigated (e.g. Durack and Wijffels, 2010; Stramma *et al*., 2010; Cai *et al*., 2015). The physical changes in the Indian Ocean are the best studied and are the best resolved through a combination of considerable observational effort and modeling. Chemical and biological studies that are sufficient to detect significant temporal trends are very scarce. The long-term trends of increasing CO_2 and decreasing O_2 at depth tend to change slowly making reasonable predictions of their trends possible from low-frequency sampling. The Bay of Bengal has a shallow low DO layer that extends south of the equator and is expanding (Stramma *et al*., 2010), with the potential to disrupt fisheries (Stramma *et al*., 2012). This low DO layer appears to be high in nitrate and CO_2, and low in pH (Waite *et al*., 2013). The seasonal dynamics of other chemical and the biological components, especially in the euphotic zone, require monthly sampling to resolve trends (Henson, 2014).

The lack of biological monitoring in the Indian Ocean severely limits our ability to understand the effects of climate variability on ecological processes and biodiversity (Dobson, 2005). In addition, the heterogenetic spatial and temporal distributions of biota can make it much more challenging to detect long-term trends or broad spatial patterns. For example, the seasonal variability in phytoplankton biomass can be significant and change annually, requiring sustained and consistent sampling to detect any type of longer-term trend. Thus, detecting a relatively small climate signal requires long-term, carefully designed sampling regimes. Trends in the basic biology of phytoplankton, primary production, zooplankton, and secondary production are known from only a few points in the Indian Ocean. More numerous are reports of significant and rapid range expansions by pelagic biota in response to the changing climate (McLeod *et al*., 2012; Sunday *et al*., 2015). The lack of fisheries-independent stock assessments, the potential for unreported fishing effort, and the instability in catch per unit effort (cpue) means that a robust measure of trends for many populations of fish species is not available at the basin scale.

In the next section, we present some of the most notable changes that have been reported in the literature for the Indian Ocean and compare them to the available data for this report using a geographic framework (Longhurst, 2007).

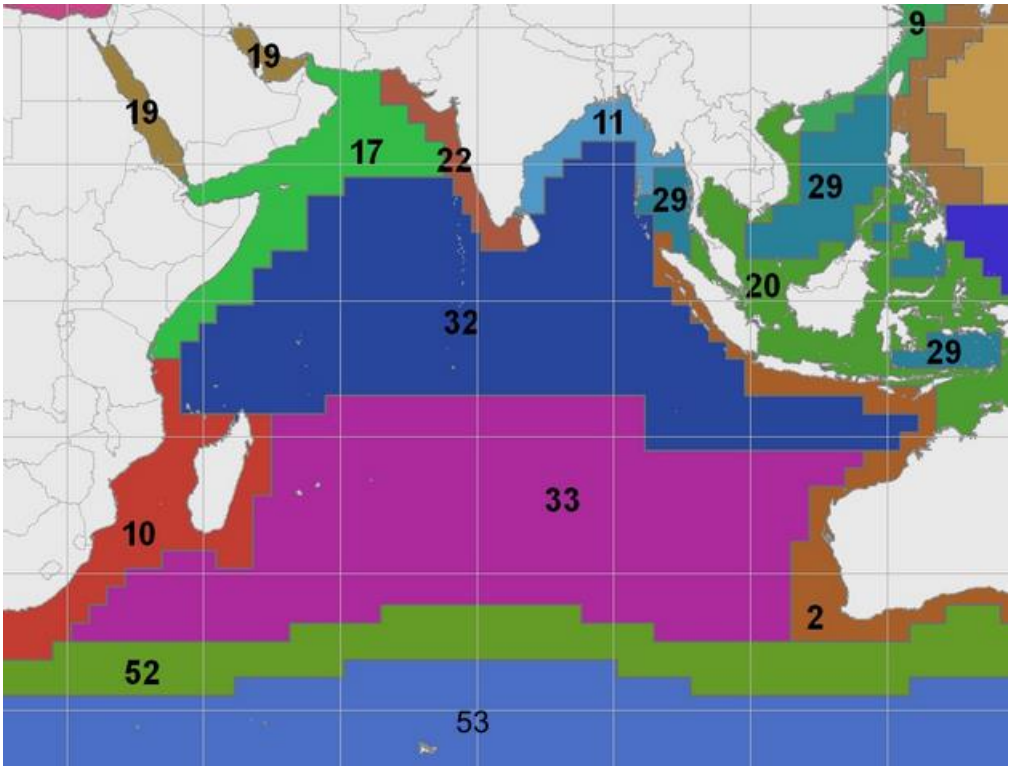

Figure 7.6. The Indian Ocean and surrounding marginal seas separated into biogeographical provinces after Longhurst (1995, 2007). The provinces are based on the types of physical forces that determine the pelagic ecology, particularly the distribution of phytoplankton (*et al*., 2013). Indian Ocean provinces include the: Northwest Arabian Upwelling (17), Red Sea and Persian Gulf (19), East Africa Coastal (10), Australia–Indonesia Coastal (2), Subtropical Convergence (52), Subantarctic (53), East India Coastal (11), West India Coastal (22), Archipelago Deep Basin (29), India Monsoon Gyres (32), and India Subtropical Gyre. (33).

7.4.1 Northwest Arabian upwelling province (Longhurst 17), Red Sea and Persian Gulf province (Longhurst 19)

A series of cruises to this region during the 1990s produced significant insights into the pelagic ecology (Smith, 2005), especially the biological responses to monsoonal forcing (Wiggert *et al*., 2005). Unfortunately, there are limited *in situ* time-series data to assess long-term ecological trends. A regional peak in satellite chlorophyll *a* was observed in 2003 associated with a negative SLA and low SST (Prakash *et al*., 2012). Similarly, a very low SST and strong upwelling was observed in 1966 (Roxy *et al*., 2016). The patchy increases in satellite chlorophyll *a* scattered across the northwest Arabian upwelling province seen over the 5- and 15-year temporal windows may reflect positive IOD and negative ENSO events during the early monsoon season (Currie *et al*., 2013). At this time, the considerable interannual variability and local effects of climate cycles make it difficult to conclude whether the region will experience a longer-term trend towards increased upwelling under prolonged climate change (Bakun, 1990; Goes *et al*., 2005; Prakash and Ramesh, 2007; Narayan *et al*., 2010; Sydeman *et al*., 2014). The significant positive chlorophyll *a* trend in the Gulf of Oman and Persian Gulf, especially observed in the 15-year time-window, is consistent with reports of large blooms of the green form of *Noctiluca scintillans* (Gomes *et al*., 2014). This mixotrophic dinoflagellate, which grows fastest when grazing, has been increasing globally (Harrison *et al*., 2011). Gomes *et al*. (2014) linked the rise in *N. scintillans* with eutrophication and indicated that it was coincident with declining subsurface dissolved oxygen. The 15-year trend of increasing satellite-detected chlorophyll *a* in the Red Sea reported herein has been investigated by Raitsos *et al*. (2015), who suggest that the physical mechanism stimulating primary production is related to ENSO climate

variability in monsoonal winds and nutrient injection from the Indian Ocean, allowing the southern Red Sea to bloom. Unfortunately, the only IGMETS time-series data available from the Red Sea is from the Gulf of Eilat in the far north and well away from this 15-year trend of increasing phytoplankton. In the Gulf of Eilat, the warming and declining nutrients are consistent with the generally expected responses to climate change (Laufkötter *et al*., 2015).

7.4.2 East Africa coastal province (Longhurst 10)

The zooplankton biomass on the Agulhas Bank has declined 57% since 1988 (J. Huggett, pers. comm.). In particular, abundance of the large calanoid zooplankton *Calanus agulhas* has decreased significantly. Available information suggests that increasing SST and predation by anchovy (*Engraulis capensis*) and sardine (*Sardinops sagax*) may be the primary causes (J. Huggett, pers. comm.), a relationship that has been observed nearby on the west coast of Africa (Verheye *et al*., 1998). Increasing SST has been frequently associated with declining populations of large macrozooplankton (Daufresne *et al*., 2009). This province has spatially heterogeneous trends in physical and ecological characteristics that are apparently associated with changing coastal boundary currents (Backeberg *et al*., 2012).

7.4.3 Australia–Indonesia coastal province (Longhurst 2)

Lower SST, greater upwelling, and more chlorophyll *a* off Java and Sumatra have been previously linked to a positive IOD and negative ENSO during September–November (Currie *et al*., 2013). Based on *in situ* data from Rottnest Island (1951–2002), a warming trend of ca. 0.012° $year^{-1}$ has been reported for the west coast of Australia (Thompson *et al*., 2009), which is consistent with the 30-year SST trend reported here. The La Niña event of 2011 was associated with a pronounced increase in water temperature (Feng *et al*., 2013), a decline in zooplankton biomass, and significantly more of the picoplankton *Prochlorococcus* and *Synechococcus*, which are most abundant in the tropics (Thompson *et al*., 2015).

7.4.4 Subtropical convergence province (Longhurst 52)

The subtropical convergence and the subtropical front separates the more saline subtropical waters from the fresher subantarctic waters. The physical drivers are spatially and temporally dynamic (Graham and de Boer, 2013).

The province stretches across the South Atlantic, Indian, and South Pacific oceans and has high eddy kinetic energy and substantial westward flow. In this report, the STF showed evidence of increased chlorophyll *a* across the South Atlantic, South Pacific, and South Indian oceans. In the Indian Ocean, it is possible that this increase is related to large blooms of coccolithophores, which occur in mid-summer (Brown and Yoder, 1994; Balch *et al*., 2011). There is evidence of a diversity of *Emiliania huxleyi* morphotypes (Cubillos *et al*., 2007; Cook *et al*., 2011) and a poleward expansion of these taxa (Winter *et al*., 2014).

7.4.5 Subantarctic province (Longhurst 53)

This province is only rarely within the 45°S limit ascribed to the Indian Ocean for the purpose of this report (Orsi *et al*., 1995). Unfortunately, *in situ* time-series data from this province and within the Indian Ocean sector are very rare. One exceptional dataset was published by Hirawake *et al*. (2005) from regular cruises between Tokyo and the Antarctic continent once a year. The authors reported an increase in chlorophyll *a* over their time series (1965–2002, a trend which is consistent with the remotely-sensed data analyzed herein.

7.5 Conclusions

The Indian Ocean had the greatest extent of warming of all oceans, with 91.8% of its area showing a significant positive trend over 30 years, compared with the Atlantic (88.6%), Pacific (65.9%), Arctic (79.2%), and Southern (31.8%) oceans. In addition to having a high degree of warming, the Indian Ocean also had the greatest proportion of its area (55.1%) showing a significant ($p < 0.05$) decline in chlorophyll *a* between 1998 and 2012. The 51 million km^2 of warming in the Indian Ocean may reflect the fact that the northern Indian Ocean is landlocked at ca. 25°N and, therefore, has no high-latitude, seasonal deep mixing to supply cold surface water.

Across the entire Indian Ocean, a few relatively small and mostly upwelling regions, previously identified as productive (Carr *et al*., 2006), have shown remarkable resilience to warming or declining chlorophyll *a* over the past 30 or 15 years, respectively. These regions off Sumatra and Java, off Somalia and Oman, in the Arabian and Red Seas, and along the STF all showed areas of temperature stability or decline and an increase in chlorophyll *a* during 1998–2012. Upwelling was predicted to intensify under global warming (Bakum, 1990), and there is evidence of this happening in the Indian Ocean. The rise in phytoplankton along the STF is consistent with some coarse-scale modeling of the ocean in 2090 (Marinov *et al*., 2013), although the mechanism and proposed taxonomic shift towards diatoms cannot be confirmed. It should be noted that these regions are the overwhelming minority of the Indian Ocean, with only 0.5% of the area tending significantly downward in temperature over 30 years and 4.8% trending significantly upward for chlorophyll *a* over a 15-year time-period.

Given the spatial scale of warming in the Indian Ocean, it seems likely that climate impacts on marine ecosystems will be most pronounced in this ocean. At the same time, the Indian Ocean has very few *in situ* biogeochemical time series that can be used to assess impacts of climate change on biota or biodiversity. The few time series that exist in the IGMETS database are all on the continental shelves of just two continents, leaving vast areas completely unmonitored. Still, new insights have arisen from examining trends over sequential time-steps and from the effort to couple physical observations with observed biological responses, including *in situ* observations. These *in situ* observations allow unprecedented insights into trends in ecology driven by climate. Previous research on ecological responses of the Indian Ocean to climate change at the basin-scale have been largely model-based (Currie *et al*., 2013), limited to trends detected by remote sensing, or a few local case studies. This IGMETS report is the first effort to bring multiple *in situ* time series together to provide a global synthesis and basin-scale comparisons of long-term trends.

Table 7.3. Time-series sites located in the IGMETS Indian Ocean region. Participating countries: Australia (au), Israel (il), and South Africa (za). Year-spans in red text indicate time series of unknown or discontinued status.

No.	IGMETS-ID	Site or programme name	Year-span	T	S	Oxy	Ntr	Chl	Mic	Phy	Zoo
1	au-10101	Swan River Estuary: S01 Blackwall Reach *(Southwestern Australia)*	1994–present	X	X	X	X	X	-	X	-
2	au-40114	SO-CPR Aurora 140-160-B4245 *(Southern Ocean)* *see Southern Ocean Annex A4)*	2008–present	X	X	-	-	X	-	-	X
3	au-40205	AusCPR MEAD Line *(Australian Coastline)* *see Southern Ocean Annex A4)*	2010–present	-	-	-	-	X	-	X	X
4	au-50102	IMOS National Reference Station Darwin *(Northern Australia)*	2011–present	X	X	-	X	X	X	X	X
5	au-50103	IMOS National Reference Station Esperance *(Southern Australia)*	2009–present	X	X	X	X	X	X	X	X
6	au-50104	IMOS National Reference Station Kangaroo Island *(Southern Australia)*	2008–present	X	X	-	X	X	X	X	X
7	au-50106	IMOS National Reference Station Ningaloo *(Western Australia)*	2010–present	X	X	-	X	X	X	X	X
8	au-50108	IMOS National Reference Station Rottnest Island *(Southwestern Australia)*	2009–present	X	X	-	X	X	X	X	X
9	il-10101	Gulf of Eilat Aqaba NMP Station A *(Gulf of Eilat – Gulf of Aqaba)*	2003–present	X	X	X	X	X	-	-	-
10	za-30202	ABCTS Mossel Bay Monitoring Line *(Agulhas Bank)*	1988–present	-	-	-	-	-	-	-	X

7.6 References

Abram, N. J., Mulvaney, R., Vimeux, F., Phipps, S. J., Turner, J., and England, M. H. 2014. Evolution of the Southern Annular Mode during the past millennium. Nature Climate Change, 4(7): 564–569.

Alory, G., Wijffels, S., and Meyers, G. 2007. Observed temperature trends in the Indian Ocean over 1960–1999 and associated mechanisms. Geophysical Research Letters, 34: L02606.

Backeberg, B. C., Penven, P., and Rouault, M. 2012. Impact of intensified Indian Ocean winds on mesoscale variability in the Agulhas system. Nature Climate Change, 2: 1–5.

Bakun, A. 1990. Global climate change and intensification of coastal ocean upwelling, Science, 247: 198–201.

Balch W. M., Drapeau D. T., Bowler B. C., Lyczkowski, E., Booth, E. S., and Alley, D. 2011. The contribution of coccolithophores to the optical and inorganic carbon budgets during the Southern Ocean Gas Exchange Experiment: new evidence in support of the "Great Calcite Belt" hypothesis. Journal of Geophysical Research, 116: C00F06.

Balch, W. M., Bates, N. R., Lam, P. J., Twining, B. S., Rosengard, S. Z., Bowler, B. C., Drapeau, D. T., *et al*. 2016. Factors regulating the Great Calcite Belt in the Southern Ocean and its biogeochemical significance. Global Biogeochemical Cycles, 30: 1124–1144, doi:10.1002/2016GB005414.

Beal, L. M., and Chereskin, T. K. 2003. The volume transport of the Somali current during the 1995 southwest monsoon. Deep-Sea Research II, 50: 2077–2089.

Beal, L. M., De Ruijter, W. P. M., Biastoch, A., and Zahn, R. 2011. On the role of the Agulhas system in ocean circulation and climate. Nature, 472(7344): 429–436.

Boebel, O., Rae, C. D., Garzoli, S., Lutjeharms, J., Richardson, P., Rossby, T., Schmid, C., *et al.* 1998. Float experiment studies interocean exchanges at the tip of Africa. EOS, 79(1): 7–8.

Brown, C. W., and Yoder, J. A. 1994. Coccolithophorid blooms in the global ocean, Journal of Geophysical Research, 99: 7467–7482.

Bryden, H. L., Beal, L. M., and Duncan, L. M. 2005. Structure and transport of the Agulhas Current and its temporal variability. Journal of Oceanography, 61: 479–492, doi:10.1007/s10872-005-0057-8.

Cai, W., Santoso, A., Wang, G., Yeh, S-W., An, S-I., Cobb, K. M., Collins, M., *et al*. 2015. ENSO and greenhouse warming. Nature Climate Change, 5: 849–859, doi:10.1038/nclimate2743.

Carr, M., Friedrichs, M. A. M., Schmeltz, M., Aita, M. N., Antoine, D., Arrigo, K. R., Asanuma, I., *et al*. 2006. A comparison of global estimates of marine primary production from ocean color. Deep-Sea Research II, 53: 741–770.

Carranza, M. M., and Gille, S. T. 2015. Southern Ocean wind-driven entrainment enhances satellite chlorophyll-a through the summer. Journal of Geophysical Research: Oceans, 120: 304–323, doi:10.1002/2014JC010203.

Cook, S. S., Whittock, L., Wright, S. W., and Hallegraeff, G. M. 2011. Photosynthetic pigment and genetic differences between two Southern Ocean morphotypes of *Emiliania huxleyi* (Haptophyta). Journal of Phycology, 47: 615–626.

Cubillos, J. C., Wright, S. W., Nash, G., de Salas, M. F., Griffiths, B., Tilbrook, B., Poisson, A., *et al*. 2007. Calcification morphotypes of the coccolithophorid *Emiliania huxleyi* in the Southern Ocean: Changes in 2001 to 2006 compared to historical data. Marine Ecological Progress Series, 348: 47–54.

Cresswell, G. R., and Griffin, D. A. 2004. The Leeuwin Current, eddies and sub-Antarctic waters off south-western Australia. Marine Freshwater Research, 55: 267–276.

Currie, J. C., Lengaigne, M., Vialard, J., Kaplan, D. M., Aumont, O., Naqvi, S. W. A., and Maury, O. 2013. Indian Ocean Dipole and El Niño/Southern Oscillation impacts on regional chlorophyll anomalies in the Indian Ocean. Biogeosciences, 10: 6677–6698.

Daufresne, M., Lengfellner, K., and Sommer, U. 2009. Global warming benefits the small in aquatic ecosystems. Proceedings of the National Academy of Sciences of the United States of America, 106: 12788–12793.

Dobson, A. 2005. Monitoring global rates of biodiversity change: challenges that arise in meeting the Convention on Biological Diversity (CBD) 2010 goals. Philosophical Transactions of the Royal Society B, 360: 229–241.

Durack, P. J., and Wijffels, S. E. 2010. Fifty-year trends in global ocean salinities and their relationship to broad-scale warming. Journal of Climate, 23: 4342–4362.

Eccles, F., and Tziperman, E. 2004. Nonlinear effects on ENSO's period. Journal of Atmospheric Science, 61: 474–482.

Falkowski, P. G., Ziemann, D., Kolber, Z., and Bienfang, P. K. 1991. Role of eddy pumping in enhancing primary production in the ocean. Nature, 352(6330): 55–58.

Feng, M., McPhaden, M. J., Xie, S., and Hafner, J. 2013. La Niña forces unprecedented Leeuwin Current warming in 2011. Scientific Reports 3: 1277, doi:10.1038/srep01277.

Fogt, R. L., Perlwitz, J., Monaghan, A. J., Bromwich, D. H., Jones, J. M., and Marshall, G. J. 2009. Historical SAM variability. Part II: twentieth-century variability and trends from reconstructions, observations, and the IPCC AR4 models. Journal of Climate, 22: 5346–5365.

Fyfe, J. C., Boer, G. J., and Flato, G. M. 1999. The Arctic and Antarctic Oscillations and their projected changes under global warming. Geophysical Research Letters, 26: 1601–1604.

Galy, V., France-Lanord, C., Beyssac, O., Faure, P., Kudrass, H., and Palhol, F. 2007. Efficient organic carbon burial in the Bengal fan sustained by the Himalayan erosional system. Nature, 450: 407–410.

Godfrey, J. S., and Ridgway, K. R. 1985. The large-scale environment of the poleward-flowing Leeuwin current, Western Australia: longshore steric height gradients, wind stresses and geostrophic flow. Journal of Physical Oceanography, 15: 481–495.

Goes, J. I., Thoppil, P. G., Gomes, H. D., and Fasullo, J. T. 2005. Warming of the Eurasian landmass is making the Arabian Sea more productive. Science, 308: 545–547.

Gomes, H. D. R., Goes, J., Matondkar, S. G. P., Buskey, E. J., Basu, S., Parab, S., and Thoppil, P. 2014. Massive outbreaks of *Noctiluca scintillans* blooms in the Arabian Sea due to spread of hypoxia. Nature Communications, 5: 4862, doi:10.1038/ncomms5862.

Gong, D., and Wang, S. 1999. Definition of Antarctic oscillation index. Geophysical Research Letters, 26: 459–462.

Graham, R. M., and De Boer, A. M. 2013. The Dynamical Subtropical Front, Journal of Geophysical Research, 118: 5676–5685, doi:10.1002/jgrc.20408.

Gregg, W. W., and Rousseaux, C. S. 2014. Decadal trends in global pelagic ocean chlorophyll: A new assessment integrating multiple satellites, in situ data, and models. Journal of Geophysical Research: Oceans, 119: 5921–5933, http://dx.doi.org/10.1002/2014JC010158.

Hall, A., and Visbeck, M. 2002. Synchronous variability in the Southern Hemisphere atmosphere, sea ice, and ocean resulting from the annular mode. Journal of Climate, 15: 3043–3057.

Han, W., Vialard, J., McPhaden, M. J., Lee, T., Masumoto, Y., Feng, M., and de Ruijter, W. P. M. 2014. Indian Ocean decadal variability: a review. Bulletin of the American Meteorological Society, 95: 1679–1703.

Harrison, P. J., Furuya, K., Glibert, P., Xu, J., Liu, H. B., Yin, K., Lee, J. H. W., *et al*. 2011. Geographical distribution of red and green *Noctiluca scintillans*. Chinese Journal of Oceanology and Limnology, 29: 807–831, doi:10.1007/s00343-011-0510-z.

Henson, S. A. 2014. Slow science: the value of long ocean biogeochemistry records. Philosophical Transactions of the Royal Society A, 372(2025), doi:10.1098/rsta.2013.0334.

Hirawake, T., Odate, T., and Fukuchi, M. 2005. Long-term variation of surface phytoplankton chlorophyll *a* in the Southern Ocean during 1965–2002. Geophysical Research Letters, 32(2005): L05606, http://dx.doi.org/10.1029/2004GL021394.

Hutchings, L., Verheye, H. M., Mitchell-Innes, B. A., Peterson, W. T., Huggett, J. A., and Painting, S. J. 1995. Copepod production in the southern Benguela system. ICES Journal of Marine Science, 52: 439–455.

Jena, B., Sahu, S., Avinash, K., and Swain, D. 2013. Observation of oligotrophic gyre variability in the South Indian Ocean: Environmental forcing and biological response. Deep-Sea Research I, 80: 1–10.

Jones, E. M., Doblin, M. A., Matear, R., and King, E. 2015. Assessing and evaluating the ocean-colour footprint of a regional observing system. Journal of Marine Systems, 143: 49–61.

Kämpf, J. 2015. Undercurrent-driven upwelling in the northwestern Arafura Sea. Geophysical Research Letters, 42: 9362–9368, doi:10.1002/2015GL066163.

Langlais, C., Rintoul, S., and Zika, J. 2015. Sensitivity of Antarctic circumpolar transport and eddy activity to wind patterns in the Southern Ocean. Journal of Physical Oceanography, 45: 1051–1067, doi:10.1175/JPO-D-14-0053.1.

Laufkötter, C., Vogt, M., Gruber, N., Aita-Noguchi, M., Aumont, O., Bopp, L., Buitenhuis, E., *et al*. 2015. Drivers and uncertainties of future global marine primary production in marine ecosystem models. Biogeosciences, 12: 6955–6984, doi:10.5194/bg-12-6955-2015.

Longhurst, A. 1995. Seasonal cycles of pelagic production and consumption. Progress in Oceanography, 36: 77–167.

Longhurst, A. 2007. Ecological Geography of the Sea, 2nd edn. Academic Press, San Diego. 542 pp.

Lovenduski, N. S., and Gruber, N. 2005. The impact of the Southern Annular Mode on Southern Ocean circulation and biology. Geophysical Research Letters, 32: L11603, doi:10.1029/2005GL022727.

Lutjeharms, J. R. E., and van Ballegooyen, R. C. 1988. The retroflection of the Agulhas Current. Journal of Physical Oceanography, 18: 1570–1583.

Marinov, I., Doney, S. C., Lima, I. D., Lindsay, K., Moore, J. K., and Mahowald, N. 2013. North–south asymmetry in the modeled phytoplankton community response to climate change over the 21st century. Global Biogeochemical Cycles, 27: 1274–1290, doi:10.1002/2013GB004599.

McLeod, D. J., Hallegraeff, G. M., Hosie, G. M., and Richardson, A J. 2012. Climate-driven range expansion of the red-tide dinoflagellate *Noctiluca scintillans* into the Southern Ocean. Journal of Plankton Research, 34: 332–337.

Meyers, G. 1996. Variation of the Indonesian throughflow and the El Niño-Southern Oscillation. Journal of Geophysical Research, 101: 12255–12263.

Meyers, G., McIntosh, P., Pigot, L., and Pook, M. 2007. The years of El Niño, La Niña, and interactions with the tropical Indian Ocean. Journal of Climate, 20: 2872–2880, doi:10.1175/JCLI4152.1.

Narayan, N., Paul, A., Mulitza, S., and Schulz, M. 2010. Trends in coastal upwelling intensity during the late 20th century. Ocean Science, 6: 815–823, doi:10.5194/os-6-815-2010.

Nieblas, A. E., Sloyan, B. M., Coleman, R., and Richardson, A. J. 2009. Variability of biological production in low wind-forced regional upwelling systems: a case study off southeastern Australia. Limnology and Oceanography, 54: 1548–1558.

Oke, P. R., and England, M. H. 2003. Oceanic response to changes in the latitude of the Southern Hemisphere subpolar westerly winds. Journal of Climate, 17: 1040–1054.

Oke, P. R., and Sakov, P. 2012. Assessing the footprint of a regional ocean observing system. Journal of Marine Systems, 105–108: 30–51.

Orsi, A. H., Whitworth III, T., and Nowlin Jr., W. D. 1995: On the meridional extent and fronts of the Antarctic Circumpolar Current. Deep-Sea Research I, 42: 641–673.

Prakash, P., Prakash, S., Rahaman, H., Ravichandran, M., and Nayak, S. 2012. Is the trend in chlorophyll-a in the Arabian Sea decreasing? Geophysical Research Letters, 39: L23605, doi:10.1029/2012GL054187.

Prakash, S., and Ramesh, R. 2007. Is the Arabian Sea getting more productive? Current Science, 92: 667–671.

Raitsos, D. E., Yi, X., Platt, T., Racault, M., Brewin, R. J. W., Pradhan, Y., Papadopoulos, V. P., *et al*. 2015. Monsoon oscillations regulate fertility of the Red Sea. Geophysical Research Letters, 42: 855–862, doi:10.1002/2014GL062882.

Reygondeau, G., Longhurst, A., Martinez, E., Beaugrand, G., Antoine, D., and Maury, O. 2013. Dynamic biogeochemical provinces in the global ocean. Global Biogeochemical Cycles, 27: 1–13, doi:10.1002/gbc.20089.

Ridgway, K. R., and Condie, S. A. 2004. The 5500-km-long boundary flow off western and southern Australia. Journal of Geophysical Research: Oceans, 109: C04017, doi:0.1029/2003JC001921.

Roxy, M. K., Modi, A., Murtugudde, R., Valsala, V., Panickal, S., Prasanna Kumar, S., Ravichandran, M., *et al*. 2016. A reduction in marine primary productivity driven by rapid warming over the tropical Indian Ocean. Geophysical Research Letters, 43: 826–833, doi:10.1002/2015GL066979.

Saji, N. H., Goswami, B. N., Vinayachandran, P. N., and Yamagata, T. 1999. A dipole mode in the tropical Indian Ocean. Nature, 401: 360–363.

Schodlok, M. P., Tomczak, M., and White, N. 1997. Deep sections through the South Australian Basin and across the Australian-Antarctic Discordance. Geophysical Research Letters, 24: 2785–2788.

Schott, F. A., Xie, S-P., and McCreary Jr., J. P. 2009. Indian Ocean circulation and climate variability. Reviews of Geophysics, 47: RG1002, doi:10.1029/2007RG000245.

Signorini, S. R., Franz, B. B., and McClain, C. R. 2015. Chlorophyll variability in the oligotrophic gyres: mechanisms, seasonality and trends. Frontiers in Marine Science, http://dx.doi.org/10.3386/fmars.2015.0001

Smith, A. L. 2005. The Arabian Sea of the 1990s: New Biogeochemical Understanding. Progress in Oceanography, 65: 113–115.

Stramma, L., Schmidtko, S., Levin, L. A., and Johnson, G. C. 2010. Ocean oxygen minima expansions and their biological impacts. Deep-Sea Research I, Oceanographic Research Papers, 57(4): 587–595.

Stramma, L., Prince, E. D., Schmidtko, S., Luo, J., Hoolihan, J. P., Visbeck, M., Wallace, D. W. R., *et al*. 2012. Expansion of oxygen minimum zones may reduce available habitat for tropical pelagic fishes. Nature Climate Change, 2: 33–37.

Sunday, J. M., Pecl, G. T., Frusher, S., Hobday, A. J., Hill, N., Holbrook, N. J., Edgar, G. J., *et al*. 2015. Species traits and climate velocity explain geographic range shifts in an ocean-warming hotspot. Ecology Letters, 18: 944–953.

Susanto, R. D., Gordon, A. L., and Zheng, Q. 2001. Upwelling along the coasts of Java and Sumatra and its relation to ENSO. Geophysical Research Letters, 28(8): 1599–1602.

Swart, N. C., Fyfe, J. C., Gillett, N., and Marshall, G. J. 2015. Comparing trends in the Southern Annular Mode and Surface Westerly Jet. Journal of Climate, 28: 8840–8859, doi:http://dx.doi.org/10.1175/JCLI-D-15-0334.1.

Sydeman, W. J., García-Reyes, M., Schoeman, D. S., Rykaczewski, R. R., Thompson, S. A., Black, B. A., and Bograd, S. J. 2014. Climate change and wind intensification in coastal upwelling ecosystems. Science, 345(6192): 77–80.

Talley, L. D., Pickard, G. L., Emery, W. J., and Swift, J. H. 2011. Descriptive Physical Oceanography: An Introduction (Sixth edn). Elsevier, Boston. 560 pp.

Thompson, D. W. J., Wallace, J. M., and Hegerl, G. C. 2000. Annular modes in the Extratropical Circulation. Part II: Trends. Journal of Climate, 13: 1018–1036.

Thompson, P. A., Baird, M. E., Ingleton, T., and Doblin, M. A. 2009. Long-term changes in temperate Australian coastal waters and implications for phytoplankton. Marine Ecology Progress Series, 384: 1–19.

Thompson, P. A., Bonham, P., Rochester, W., Doblin, M. A., Waite, A. M., Richardson, A., and Rousseaux, C. 2015. Climate variability drives plankton community composition changes: an El Niño to La Niña transition around Australia. Journal of Plankton Research, 37(5): 966–984, doi:10.1093/plankt/fbv069.

Thompson, P. A., Wild-Allen, K., Lourey, M., Rousseaux, C., Waite A. M., Feng, M., and Beckley, L. E. 2011. Nutrients in an oligotrophic boundary current: Evidence of a new role for the Leeuwin Current. Progress in Oceanography, 91: 345–359.

Tomczak, M., and Godfrey, J. S. 2003. Regional Oceanography: an Introduction. Daya Publishing House, Delhi, India. 390 pp.

Verdy, A., Marshall, J., and Czaja, A. 2006. Sea surface temperature variability along the path of the Antarctic Circumpolar Current, Journal of Physical Oceanography, 36: 1317–1331.

Verheye, H. M., Richardson, A. J., Hutchings. L., Marska. G., and Gianakouros, D. 1998. Long-term trends in the abundance and community structure of coastal zooplankton in the southern Benguela system, 1951–1996. South African Journal of Marine Science, 19: 317–332.

Waite, A. M., Rossi, V., Roughan, M., Tilbrook, B., Thompson, P. A., Feng, M., Wyatt, A. S. J., *et al*. 2013. Formation and maintenance of high-nitrate, low pH layers in the Eastern Indian Ocean and the role of nitrogen fixation. Biogeosciences, 10: 5691–5702.

Weiqing, H., Vialard, J., McPhaden, M. J., Lee, T., Masumoto, Y., Feng, M., and de Ruijter, W. P. M. 2014. Indian Ocean decadal variability: a review. Bulletin of the American Meteorological Society, 95: 1679–1703.

Wiggert, J. D., Hood, R. R., Banse, K., and Kindle, J. C. 2005. Monsoon-driven biogeochemical processes in the Arabian Sea. Progress in Oceanography, 65: 176–213, doi: 10.1016/j.pocean.2005.03.008.

Winter, A., Henderiks, J., Beaufort, L., Rickaby, R. E. M., and Brown, C. W. 2014. Poleward expansion of the coccolithophore *Emiliania huxleyi*. Journal of Plankton Research, 36: 316–325.

Wyrtki, K. 1962. The upwelling in the region between Java and Australia during the south-east monsoon. Marine Freshwater Research, 13: 217–225.

Yamagata, T., Behera, S. K. Rao, S. A., Guan, Z., Ashok, K., and Saji, H. N. 2003. Comments on dipoles, temperature gradient, and tropical climate anomalies. Bulletin of the American Meteorological Society, 84: 1418–1422.

Yamagami, Y., and Tozuka, T. 2015. Interannual variability of South Equatorial Current bifurcation and western boundary currents along the Madagascar coast, Journal of Geophysical Research: Oceans, 120: 8551–8557.

Yi, B., Yang, P., Dessler, A., and da Silva, A. M. 2015. Response of aerosol direct radiative effect to the East Asian Summer Monsoon. IEEE Geoscience and Remote Sensing Letters, 12(3): 597–600.